M Shafiqur Rahman and Uttam K. Chakravarty*

Design and Analysis of a Hybrid Solar and Vibration Energy Harvester

https://doi.org/10.1515/ehs-2019-0006

Abstract: The performance of the small-scale stand-alone energy harvesters can be improved by implementing a hybrid energy harvesting technique. This paper aims at presenting the design and characterization of a hybrid energy harvester that can simultaneously harvest energy from mechanical vibration and solar radiation by combining piezoelectric, electromagnetic, electrostatic, and photovoltaic mechanisms. The hybrid device consists of a small high-efficiency solar panel and a bimorph PZT cantilever beam having a cylindrical tip magnet and two sets of capacitors (comb electrodes) attached on two sides of an ASTM 6061 T-6 Aluminum substrate. All the transducing sections of the configuration are interconnected by a smart hybrid electric circuit having a common optimum load resistance, an energy storage, and a microcontroller to generate and store combined power output when subjected to transverse vibration and solar radiation. The initial bias-voltage input required for the electrostatic mechanism is either obtained from the photovoltaic system or taken from the storage through the microcontroller. Results for the maximum power output are obtained at the fundamental resonance frequency of the vibrating cantilever beam. As the hybrid design allows a combined power harvesting method, more power is generated with better conversion efficiency than those obtained by stand-alone mechanisms. In addition to the power calculation, the study includes a stress and fatigue analysis of the cantilever beam using the finite element method to investigate the stress-life criteria of the hybrid structure.

Keywords: hybrid energy harvester, photovoltaic panel, piezoelectric technique, electromagnetic mechanism, electrostatic mechanism, efficiency, fatigue

***Corresponding author: Uttam K. Chakravarty,** Department of Mechanical Engineering, The University of New Orleans, 2000 Lakeshore Drive, New Orleans, LA 70148, USA,
E-mail: uchakrav@uno.edu
M Shafiqur Rahman, Department of Mechanical Engineering, The University of New Orleans, 2000 Lakeshore Drive, New Orleans, LA 70148, USA, E-mail: mrahman3@uno.edu

Introduction

Energy harvesting, also known as power harvesting, is the process of scavenging energy from ambient sources and storing that in a consumable form, typically, in the form of electrical energy. The recent development of autonomous and self-powered electronic systems is momentously facilitated by the technology of energy harvesting as it eliminates the drawbacks of the battery-dependent electronics (Ahmed, Mir, and Banerjee 2017). As a matter of fact, significant researches on energy harvesting have been going on over the last few decades (Ahmed, Mir, and Banerjee 2017; Roundy 2003; Rantz and Roundy 2017; Lee et al. 2016; Priya et al. 2017; Davidson and Mo 2014). This increase in research is invigorated by the modern advancements in low-power electronics such as the microelectromechanical systems (MEMS) and wireless technology such as wireless sensor networks (WSNs) (Priya et al. 2017). Applications of these electronic devices can be vigorously found in the fields of sensing and actuation, surveillance, biomedical science, animal migration tracking, structural health monitoring (Davidson and Mo 2014), aerospace and automobile engineering, and so on. In most cases, the low-powered wireless sensors and portable electronic devices are powered by conventional batteries which create complications such as limited lifespan, bulky weight, and maintenance issues including periodical recharging. Moreover, an environmental hazard can also be caused by the disposal of chemical batteries. Therefore, it becomes incumbent to find an effective alternative to the battery or similar nonregenerative sources for achieving the full benefits of the self-powered MEMS and wireless sensors nodes. An energy harvester (EH) is intuitively that alternative as it can extract energy from the ambient environment and can ensure an extended lifespan of the power supply by not only replacing the batteries but also recharging them.

In recent years, studies on energy harvesting from the ambient sources to power the low-powered electronic devices has gained excessive attention. The typical power requirement for the duty-cycled commercial WSNs ranges from 100 μW to 1 mW (Waterbury and Wright 2013) which can be extracted from the renewable energy sources such as, solar, (Sharma, Haque, and Jaffery 2018; Miles, Hynes, and Forbes 2005; Sivula 2015; Lewis, Zhang, and Jiang

Published online December 17, 2019

2009; Grover, Nehra, and Kedia 2019), thermal (Al-Haik, Alothman, and Hajj 2018; Chavez et al. 2017), wind, hydroelectric, radio frequency (Sample and Smith 2009), and kinetic energy (including mechanical vibration and human locomotion) (Castagnetti 2011; Lee and Tovar 2013; Yuan et al. 2018). Among all the energy sources, solar energy and mechanical vibration are two of the most prolific ones that can be utilized while designing an efficient EH (Rahman 2016). Based on these two energy sources, significant number of investigations on the stand-alone EHs were reported by the researchers employing the photovoltaic (PV) (Sharma, Haque, and Jaffery 2018; Miles, Hynes, and Forbes 2005; Sivula 2015; Lewis, Zhang, and Jiang 2009; Grover, Nehra, and Kedia 2019), piezoelectric (PE) (Erturk and Inman 2008, 2009; De Pasquale, Somà, and Fraccarollo 2012; Zhang 2014; Hwang et al. 2015; Wang, Kobayashi, and Lee 2015; Cui et al. 2015; Jiang et al. 2015; Luo et al. 2016; Kang et al. 2016; Wurpts, Twiefel, and Brouet 2017), electromagnetic (EM) (Waterbury and Wright 2013; Glynne-Jones et al. 2004; Arnold 2007; Beeby, Tudor, and White 2006; Moss et al. 2015; Yildirim et al. 2017; Zhu et al. 2019), electrostatic (ES) (Roundy, Wright, and Rabaey 2003; Mitcheson et al. 2004; Tao et al. 2015; Khan and Qadir 2016), and magnetostrictive (Zhang 2011; Liu et al. 2015) transduction mechanisms. Due to simplicity in design and ability to obtain higher power densities, the PE technique is extensively used in standalone vibration energy harvesting. In addition to the PE technique, vibration EHs based on stand-alone EM or ES mechanism were also heavily investigated by many researchers at micro and meso scales. However, studies showed that a small-scale (e. g. micro scale) EH applying only one mechanism hardly provide necessary energy even for a microelectronic device. Therefore, a smart and expedient way to increase the power density and hereby improve the efficiency of the conventional EHs is the development of a hybrid energy harvester (HEH) that incorporates multi-transduction mechanisms at a time (Rahman 2016; Challa, Prasad, and Fisher 2009; Khaligh, Zeng, and Zheng 2010; Yang et al. 2010; Shan et al. 2013; Larkin and Tadesse 2013; Chen, Cao, and Xie 2015; Xu et al. 2016; Khan and Izhar 2016; Edwards, Aw, and Hu 2015; Su et al. 2016; Xu et al. 2017; Khbeis, McGee, and Ghodssi 2009; Eun et al. 2014; Madinei et al. 2016; Gambier et al. 2012; Goudarzi, Niazi, and Besharati 2013; Yu et al. 2014; Colomer-Farrarons et al. 2011; Rahman and Chakravarty 2018).

The concept of the hybrid energy harvesting can be illustrated into two points of view – harvesting from single source (e. g. vibration) and harvesting from several sources (e. g. vibration, solar, and thermal energy) (Rahman 2016). However, one of the most common types of HEH is the one that harvests energy from the same source, e. g. vibration-based hybrid piezo-electromagnetic harvesters (Challa, Prasad, and Fisher 2009; Khaligh, Zeng, and Zheng 2010; Yang et al. 2010; Shan et al. 2013; Larkin and Tadesse 2013; Chen, Cao, and Xie 2015; Xu et al. 2016; Khan and Izhar 2016; Edwards, Aw, and Hu 2015; Su et al. 2016; Xu et al. 2017). Challa, Prasad, and Fisher (2009), Khaligh, Zeng, and Zheng (2010), Yang et al. (2010), Shan et al. (2013), and Larkin and Tadesse (2013) investigated such types of HEHs that combine piezoelectric and electromagnetic mechanisms. More advancements on the hybrid piezo-electromagnetic EHs can be attributed to the investigations of Chen, Cao, and Xie (2015), Xu et al. (2016), Khan and Izhar (2016), Edwards, Aw, and Hu (2015), Su et al. (2016), and Xu et al. (2017) where attempts were taken to increase the power output. Design and characterization of the combined piezoelectric and electrostatic EHs (Khbeis, McGee, and Ghodssi 2009; Eun et al. 2014; Madinei et al. 2016) were studied by several researchers including Khbeis, McGee, and Ghodssi (2009), Eun et al. (2014), and Madinei et al. (2016) where simultaneous transductions of piezoelectric and electrostatic technique showed promising outcomes. Gambier et al. (2012) developed an effective multifunctional energy harvesting system which was able to successfully harvest the ambient energy combining the piezoelectric, photovoltaic, and thermoelectric methods. Goudarzi, Niazi, and Besharati (2013) offered a hybrid energy harvesting technique by simultaneous exploitation of the pyroelectric and piezoelectric effects. To take advantage from both light and vibration energy sources, a hybrid indoor ambient light and vibration energy harvester was presented by Yu et al. (2014) where low light illumination was captured by a small-scale amorphous-silicon solar panel. Colomer-Farrarons et al. (2011) presented a hybrid system combining photovoltaic, piezoelectric, thermoelectric, and electromagnetic mechanisms which could deliver more power than a stand-alone EH. Again, a hybrid energy harvesting technique based on solar radiation and mechanical vibration was proposed by Rahman and Chakravarty (2018), where the self-energized hybrid device combined the photovoltaic, piezoelectric, electromagnetic, and electrostatic mechanisms for simultaneous energy harvesting. All these studies showed that, the HEHs offer greater power output than the stand-alone harvesters because of their high energy-density, multi-functionality, and a wide range of frequency bandwidth. However, further studies are required on the efficient hybridization techniques to obtain better efficiency than the existing hybrid systems.

In this study, a HEH is designed and analyzed that can scavenge energy from mechanical vibration and solar radiation without any power supply from nonregenerative

sources such as, batteries or fuel cells. This device offers increased power output and good efficiency as it combines the output obtained from the PV, PE, EM, and ES mechanisms simultaneously. A combined EH circuit operating at 5 V is designed in Proteus 8.6. The mathematical model of the hybrid energy harvester is coded and solved in MATLAB R2015a and the modal and structural analyses are conducted in ANSYS Workbench 15.0 using finite element (FE) method. Results for power outputs from the PE, EM, and ES mechanisms are obtained at the fundamental natural frequency of the hybrid beam using 1 g base excitation. As the hybrid structure is subjected to transverse vibration, it considers the necessity of the fatigue analysis to verify the structural reliability of the structure. Therefore, the fatigue behavior of the hybrid beam is also determined by conducting the FE analysis and studying the standard Stress-Life Curves (S-N Curves) for the base material of the structure, i. e. the aluminum substrate of the HEH model.

Design of the Hybrid Energy Harvester

Hybrid Cantilever Beam

The HEH consists of a bimorph Lead Zirconate Titanate (PZT) cantilever beam having a 6061-T6 Aluminum (Al) substrate and a cylindrical NdFeB magnet as a tip mass. The cylindrical magnet is surrounded by an induction coil of 1200 turns which is coaxially configured with the magnet on a frame. The volume of the Al substrate is 100 mm × 10 mm × 0.75 mm while each of the PZT layers have a volume of 90 mm × 8 mm × 0.40 mm. The PZT layers operate in d_{31} mode (i. e. with transverse piezoelectric strain coefficient) as the beam vibrates in transverse direction. Two sets of copper electrodes, in the shape of a hair comb, are attached on two sides of the Al substructure by keeping insulations in between. When the beam undergoes harmonic excitation, they act as the variable capacitance electrodes (C_{var} electrodes). The PZT layers and the two sets of C_{var} electrodes are assumed to be perfectly bonded to the Al substrate. A simplified two-dimensional view of the configuration is shown in Figure 1 while the actual three-dimensional configuration is demonstrated in Figures 2 and 3.

Each set of comb-shaped C_{var} electrodes contains 70 electrodes, each having the dimension of 9 mm × 0.75 mm × 0.3 mm. The gap between two successive C_{var} electrodes in the comb is 1.1 mm (Rahman and Chakravarty 2018). Two sets of similar combs of electrodes (fixed or, stationary capacitors) are attached with the base on two sides of the beam where each electrode has the dimension of 10 mm × 1 mm × 0.2 mm. This is illustrated in Figure 2(b) where the fixed electrodes are complementing the C_{var} electrodes by fitting into the gaps. When the fixed electrodes and C_{var} electrodes overlap, the gap between the electrodes is 0.45 mm as shown in Figure 3. Since the beam oscillates in transverse direction, this gap is assumed to be constant throughout the electrostatic power generation. Among the three fundamental electrostatic configurations – in-plane overlap varying, in-plane gap closing, and out-of-plane gap closing, the third one is selected for this design to avoid contacts between the moving and stationary electrodes. The relative motion between the precharged moving capacitors and stationary capacitors governs the electrostatic transduction.

The geometric and physical properties of the HEH considered for the analysis are shown in Table 1. The

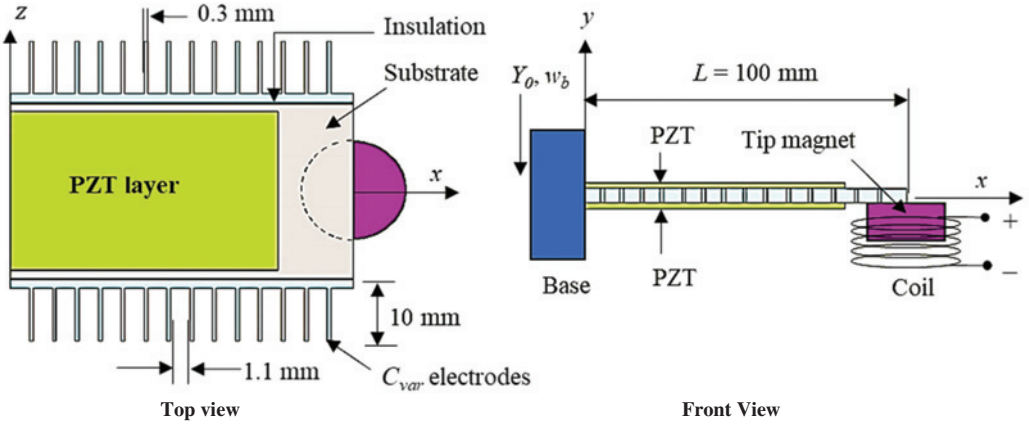

Figure 1: Schematic diagram of the hybrid cantilever beam showing top and front views (figure not drawn to scale).

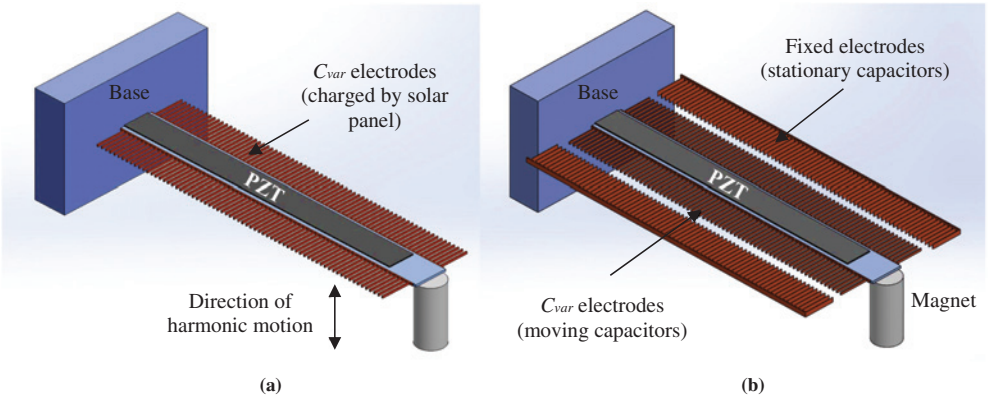

Figure 2: (a) Configurations of the 3-D hybrid energy harvester without the fixed electrodes, (b) exploded 3-D view of the hybrid structure showing the sets of fixed electrodes on two sides of the beam.

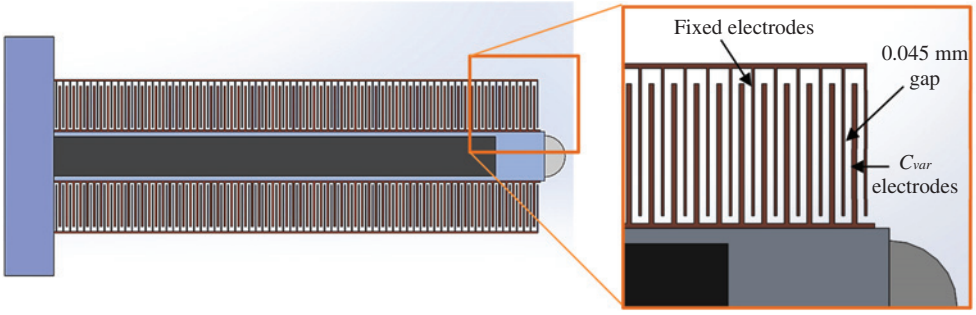

Figure 3: Top view of the hybrid energy harvester showing the details of fixed and C_{var} electrodes.

hybrid structure of the device is scalable and tunable. The tip mass and the length of the comb electrodes can be adjusted to operate at the resonance frequency (Rahman and Chakravarty 2018; Challa, Prasad, and Fisher 2011; Chen, Yang, and Deng 2009). Since the performance of the EH is sensitive to the smallest amount of change of its geometry (Yi, Shih, and Shih 2002), attention must be paid to the effective scaling of the design.

Photovoltaic Panel

The PV panel includes an array of 10 high-efficiency monocrystalline solar cells as shown in Figure 4. The size of the PV unit is 55 mm × 55 mm × 3 mm weighing 36 grams. The item number of PV panel is KS-M5555 which is selected from the China Solar LTD (http://www.solars-china.com/solar-panel/5v-80mA-oem-solar-panel.html). The data sheet information is available in the manufacturer's website (http://www.solars-china.com/solar-panel/5v-80mA-oem-solar-panel.html). The output from the PV panel is DC while the PE, EM, and ES outputs are AC outputs. Therefore, the AC outputs need to be rectified to DC outputs in the combined circuit. The HEH is designed in such a way that it allows freedom of customization of the PV panel based on the power requirement (e. g. using different scale or type) because the PV panel is not an integrated part of the hybrid cantilever beam. However, the power (bias input) supplied to the C_{var} electrodes form the PV panel must be adequate to excite the electrodes in order to generate electrostatic power output.

The operating voltage and current of the PV panel are 5 V and 80 mA, respectively. The other important specifications are shown in Table 2.

A Hybrid Power Conditioning Circuit

A simplified circuit diagram of the proposed HEH is shown in Figure 5 where the PV, ES, PE, and EM generators are parallelly connected to operate at 5 V. The PV panel generates DC while the vibration-based methods induce AC which must be converted to DC by rectifiers when combined with the PV generator. Voltage regulators maintain a constant operating voltage of 5 V. The

Table 1: Geometric and physical parameters of the hybrid cantilever beam (Rahman 2016; Rahman and Chakravarty 2018).

Parameter	Value
Length of the cantilever beam, L	100 mm
Length of the PZT layer, L_p	90 mm
Length of the comb-electrodes, L_e	100 mm
Height and Width of the substrate, h_s and b_s	0.75 mm and 10 mm
Height and width of each PZT layer, h_p and b_p	0.4 mm and 8 mm
Piezoelectric strain constant, e_{31}	$-13.74\ C/m^2$
Dielectric permittivity of the PZT layer, ε_{33}^s	6.46 nF/m
Height and effective width of the comb-electrodes, h_e and b_e	0.75 mm and 2.9 mm
Area moment of inertia of the beam, I_c	$0.001066\ m^4$
Height and radius of the magnet	20 mm and 4.2 mm
Number of turns and height of the coil	2000 and 25 mm
Inner and outer radii of the coil	5.2 mm and 7.2 mm
Length, l and radius of the coil wire	12 m and 0.0615 mm
Distance between the coil and the magnet, d	1 mm
Magnetic flux density, B	1.18 T
Density of comb electrodes, ρ_e	$8960\ kg/m^3$
Density of PZT, ρ_p	$7800\ kg/m^3$
Density of the substrate, ρ_s	$2700\ kg/m^3$
Density of the magnet, ρ_m	$7400\ kg/m^3$
Young's modulus of comb electrodes, E_e	117 Gpa
Young's modulus of PZT, E_p	66 GPa
Young's modulus of substrate, E_s	70 GPa
Young's modulus of the magnet, E_m	160 GPa

Table 2: Specifications of the PV panel (http://www.solars-china.com/solar-panel/5v-80mA-oem-solar-panel.html).

Parameter	Value
Open circuit voltage, V_{OC}	6 V
Short circuit current, I_{SC}	87 mA
Maximum power, P_{PV}	0.4 W
Nominal operating cell temperature	45 ± 2 °C
Temperature coefficient of I_{SC}	(0.045 ± 0.01) %/°C
Temperature coefficient of V_{OC}	−(0.34 ± 0.01) %/°C
Temperature coefficient of power	−(0.47 ± 0.05) %/°C
Efficiency, η_{Solar}	≥17 %
Operating temperature	−40 °C to 85 °C

combined current passes through a microcontroller that decides where to pass the current through a load resistance or to store it in a low voltage (e. g. 3.6 V) battery. The microcontroller also plays an important role in biasing the ES system by supplying a portion of the harvested

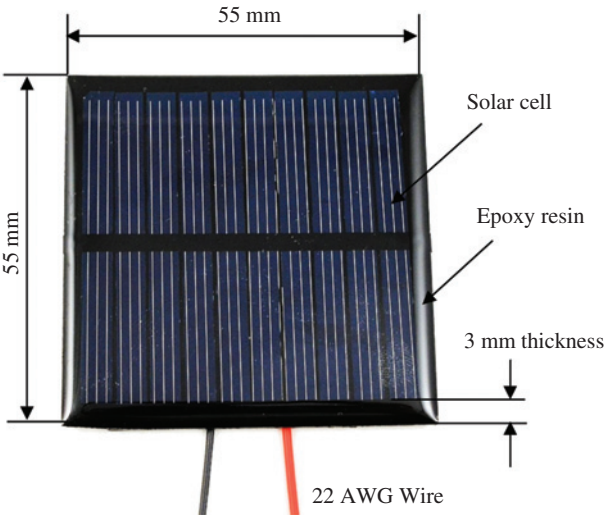

Figure 4: Configuration of the 5 V 80 mA solar panel (Item no: KS-M5555) (http://www.solars-china.com/solar-panel/5v-80mA-oem-solar-panel.html).

energy or charge from the battery to the C_{var} electrodes. If the harvested power is low, the battery will provide the back-up power to the load resistance through the microcontroller. The design of the power harvesting circuit thus allows a continuous power supply to the MEMS and WSNs even though the solar energy or mechanical vibration is inadequate or absent.

Mathematical Model

The mathematical model of the proposed HEH is developed including the photovoltaic equations and the governing partial differential equation of a vibrating cantilever beam with a tip mass in a distributed parameter system (Rahman 2016; Rahman and Chakravarty 2018). Under a small-amplitude harmonic excitation, the Euler–Bernoulli beam theory is applicable to the hybrid beam. Therefore, the shear deformation and rotary inertia of the beam are neglected. Expressions of power output are presented for each mechanism and finally, the total power output and efficiency formulations are derived.

Photovoltaic Equations

Considering a PV array with N_S number of cells in series and N_P number of strings in parallel. the output current I

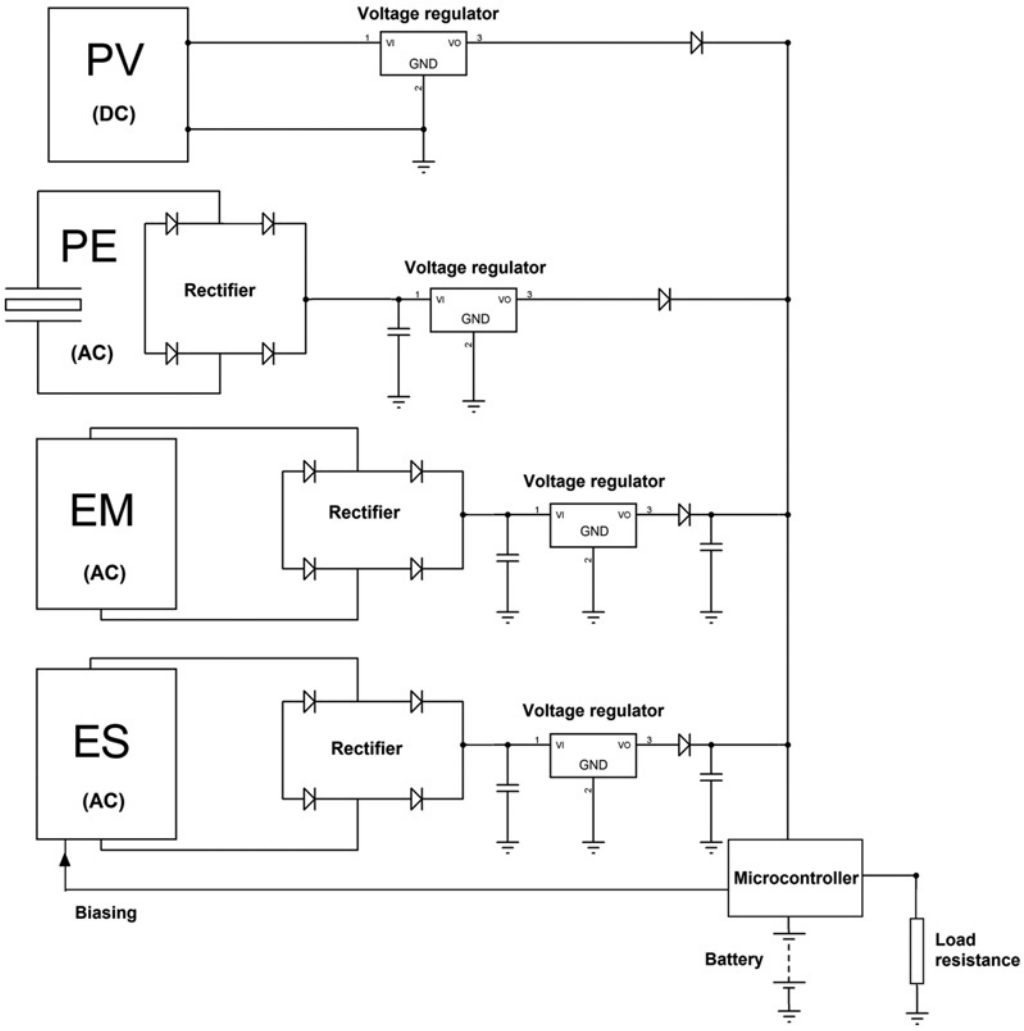

Figure 5: Schematic diagram of the combined circuit of the hybrid energy harvester.

and output voltage V can be obtained from eqs. (1)–(4) (Rahman and Chakravarty 2018; Sood and Bhalla 2013).

$$I = N_P I_{PH} - N_P I_S \left[\exp\left(\frac{q(V/N_S + IR_S)}{N_p/kT_C A}\right) - 1\right] - \frac{(N_p V/N_s + IR_s)}{R_{SH}} \quad (1)$$

where I_{PH} is the light-generated current or photocurrent, I_S is the cell saturation of dark current, $q = 1.6 \times 10^{-19}$ C is the electron charge, $k = 1.38 \times 10^{-23}$ J/K is Boltzmann's constant, T_c is the cell's working temperature, A is diode's ideality factor (typically between 1 and 2), R_{SH} is the shunt resistance, and R_S is the series resistance. The photocurrent I_{PH} can be calculated as follows:

$$I_{PH} = \left[I_{SC} + K_1\left(T_C - T_{ref}\right)\right]\lambda \quad (2)$$

where I_{SC} is the short-circuit current of a cell at reference temperature of 25 °C and reference irradiance of 1000 W/m^2, $K_1 = 0.032$ is the cell's short-circuit current temperature coefficient (Sood and Bhalla 2013), T_{ref} is the cell's reference temperature, and λ is the solar insolation (irradiance) in W/m^2. The cell's saturation current varies with the change in cell temperature, which is expressed as

$$I_S = I_{RS}\left(\frac{T_C}{T_{ref}}\right)^3 \exp\left[\frac{qE_G\left(\frac{1}{T_{ref}} - \frac{1}{T_C}\right)}{kA}\right] \quad (3)$$

where I_{RS} is the cell's reverse saturation current at a reference temperature and irradiance, and E_G is the band energy of the semiconductor used in the cell. The reverse saturation current I_{RS} at the reference temperature can approximately be obtained as

$$I_{RS} = \frac{I_{SC}}{\left[exp\left(\frac{qV_{OC}}{N_s kT_C A}\right) - 1\right]} \tag{4}$$

Several parameters including the open-circuit voltage, V_{OC} (at $I = 0$), short-circuit current, I_{SC} (at $V = 0$), and the fill factor (FF) determine the performance of a solar cell, which are related as

$$FF = \frac{I_{mp}V_{mp}}{I_{SC}V_{oc}} = \frac{P_{pv}}{I_{SC}V_{oc}} \tag{5}$$

where I_{mp} and V_{mp} are the current and voltage operating points for the maximum power P_{pv}, respectively. The output power is calculated by taking the product of either I and V, or, I^2 and R_L (Rahman and Chakravarty 2018). However, in terms of the FF, the maximum PV power output is determined by

$$P_{pv} = FF \times I_{SC}V_{OC} \tag{6}$$

Piezoelectric Equations

Assuming the Euler-Bernoulli beam, the coupled electromechanical equation for a bimorph PZT cantilever beam of length L with a tip mass M_t and mass per unit length m_L can be represented as follows (Rahman 2016; Erturk and Inman 2008; Rahman and Chakravarty 2018):

$$\begin{aligned} &E_cI_c\frac{\partial^4 w_{rel}(x,t)}{\partial x^4} + C_sI_c\frac{\partial^5 w_{rel}(x,t)}{\partial x^4 \partial t} + C_a\frac{\partial w_{rel}(x,t)}{\partial t} \\ &+ m_L\frac{\partial^2 w_{rel}(x,t)}{\partial t^2} + \vartheta V(t)\left[\frac{d\delta(x)}{dx} - \frac{d\delta(x-L)}{dx}\right] \\ &= -\left[m_L + M_t\delta(x-L)\right]\frac{\partial^2 w_b(x,t)}{\partial t^2} \end{aligned} \tag{7}$$

Here, C_sI_c is the internal (Kelvin-Voigt) damping and C_a is the viscous air damping. The sum of the harnonic base displacement $w_b\left(= Y_0 e^{j\omega t}\right)$ and relative displacement w_{rel} gives the total transverse displacement w at any time t and location x of the beam as follows:

$$w(x,t) = w_b(x,t) + w_{rel}(x,t) \tag{8}$$

The electromechanical coupling term ϑ for series connection of bimorph PZT is given by

$$\vartheta = \frac{e_{31}b}{2h_p}\left[\frac{h_s^2}{4} - \left(h_p + \frac{h_s}{2}\right)^2\right] \tag{9}$$

where e_{31} is the piezoelectric strain constant. The vibration response relative to the base can be represented as a convergent series of the Eigen functions by following modal damping (Erturk and Inman 2008, 2009; Rahman and Chakravarty 2018) as follows:

$$w_{rel}(x,t) = \sum_{n=1}^{\infty}\phi_n(x)\eta_n(t) \tag{10}$$

where $\emptyset_n$ and η_n are the mass normalized Eigen function and the modal coordinate of the clamped-free beam for the n^{th} mode, respectively. Now, the governing equation indicates that, four boundary conditions are required in terms of x and two initial conditions are needed in terms of t for the solution (Rahman and Chakravarty 2018). At the fixed end (i. e. $x = 0$),

$$w_{rel} = 0, \frac{\partial w_{rel}}{\partial x} = 0 \tag{11}$$

At the free end (i. e. $x = L$), moment M is zero, but shear force is equal to the applied force F_n at the tip, i. e.

$$M = E_cI_c\frac{\partial^2 w_{rel}}{\partial x^2} = 0 \tag{12}$$

$$F_n = \frac{\partial}{\partial x}\left(E_cI_c\frac{\partial^2 w_{rel}}{\partial x^2}\right) = m_{eff}g \tag{13}$$

where m_{eff} represents the effective mass of the hybrid beam and g is the gravitational acceleration. The modal mechanical response η_n can be obtained from the mass normalized reduced partial differential equation as follows:

$$\ddot{\eta_n}(t) + 2\zeta_n\omega_n\dot{\eta_n}(t) + {\omega_n}^2\eta_n(t) + \chi_n V(t) = f_n(t) \tag{14}$$

Here, f_n is the mass normalized tip force on the beam. The backward modal electromechanical coupling term χ_n can be given by

$$\chi_n = \vartheta\frac{d\phi_n(x)}{dx} \tag{15}$$

Applying the Kirchhoff laws to the circuit depicted in Figure 6, the capacitance C_P and piezoelectric current

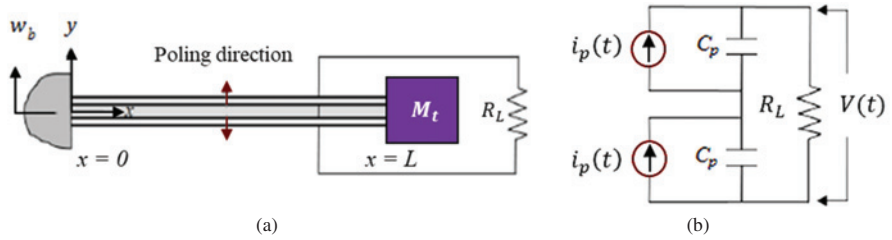

Figure 6: (a) Series connection of the two PZT layers and, (b) electrical circuit corresponding to the series connection (Erturk and Inman 2008, 2009).

$i_p(t)$ for the series connection of the PZT layers (Rahman and Chakravarty 2018) can be obtained by

$$\frac{C_P}{2}\frac{dV(t)}{dt} + \frac{V(t)}{R_L} = i_p(t) \tag{16}$$

where the capacitance and the piezoelectric current for each layer of PZT can be defined as,

$$C_P = \frac{\varepsilon_{33}^s b_p L_p}{h_p} \tag{17}$$

$$i_p(t) = \sum_{n=1}^{\infty} \varphi_n \frac{d\eta_n(t)}{dt} \tag{18}$$

In eq. (17), ε_{33}^s is the dielectric permittivity of the PZT layer for the series connection.

The forward modal coupling term φ_n can be expressed as,

$$\varphi_n = -\frac{e_{31} b (h_p + h_s)}{2}\frac{d\emptyset_n(x)}{dx} \tag{19}$$

The cross-section of the hybrid beam through the C_{var} electrodes in *y-z* plane is shown in Figure 7.

The equivalent bending stiffness E_cI_c and the mass of the beam m without the tip mass can be given by,

$$E_cI_c = \left[\frac{E_s}{24} b_s (h_s)^3 + \frac{E_p}{24}\left\{b_p (2h_p + h_s)^3 - b_p {h_s}^3\right\} + 2\frac{E_e}{24} b_e h_s^3\right] \times 2 \tag{20}$$

$$m = \rho A_{cross} L = \rho_s b_s h_s L_s + 2\rho_p b_p h_p L_p + 2\rho_e b_e h_s L_e \tag{21}$$

Therefore, the fundamental natural frequency ω_n of the hybrid beam can be found by,

$$\omega_n = \sqrt{\frac{k_{eff}}{m_{eff}}}$$

$$= \sqrt{\frac{\frac{3E_cI_c}{L^3}}{0.236\ m + M_t}}$$

$$= \sqrt{\frac{6\left[\left[\frac{E_s}{24} b_s (h_s)^3 + \frac{E_p}{24}\left\{b_p (2h_p + h_s)^3 - b_p {h_s}^3\right\} + 2\frac{E_e}{24} b_e h_s^3\right]\right]}{\left[0.236\left(\rho_s b_s h_s L + 2\rho_p b_p h_p L_p + 2\rho_e b_e h_s L\right) + M_t\right] L^3}} \tag{22}$$

where the effective stiffness and effective mass of the beam are $k_{eff} = 3EI/L^3$ and $m_{eff} = 0.236\ m + M_t$, respectively (Rahman and Chakravarty 2018). The maximum output power is obtained at the resonance condition, i. e. at $\omega = \omega_n$. The expression of power output $P_{PE}(\omega)$ for the PE generator at resonance can be given by eq. (23) (Rahman and Chakravarty 2018; Cottone 2011).

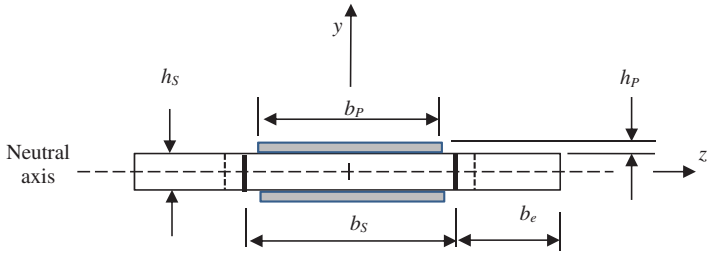

Figure 7: Cross-section of the beam through the C_{var} electrodes.

$$|P_{PE}(\omega)| = \frac{V^2(t)}{R_L} = \frac{R_L(\omega\varphi_n F_n)^2}{\left[\omega_n^2 - \omega^2(1+2\zeta_n\omega_n R_L C_P)\right]^2 + \left[2\zeta_n\omega_n\omega + \omega R_L\left[C_P(\omega_n^2-\omega^2)+\varphi_n\chi_n\right]\right]^2} \quad (23)$$

where R_L is the load resistance and ζ_n is the damping ratio of the bimorph PZT cantilever beam. At resonance, F_n is equal to resonance-equivalent static load (Challa, Prasad, and Fisher 2009) at the tip, i. e. $F_n = F_{tip} = (m + M_t)g/2\zeta_n$.

Electromagnetic Equations

The expression for the maximum EM power output $P_{EM}(\omega)$ at the resonance frequency (Rahman and Chakravarty 2018; Cottone 2011; Kim et al. 2010) is given by the following equation:

$$|P_{EM}(\omega)| = \frac{{Y_0}^2}{2R_L}\left[\frac{m_{eff}\delta_c\omega_c{\omega_n}^2\omega}{\sqrt{\left(k_{eff}\omega_c - m_{eff}\omega_c\omega^2 - d\omega^2\right)^2 + \left(k_{eff}\omega - m_{eff}\omega^3 + d\omega_c\omega + \alpha\delta_c\omega_c\omega\right)^2}}\right]^2 \quad (24)$$

where the electrical coupling force factor α, characteristic cut-off frequency ω_c, electromechanical conversion factor δ_c, and coil self-inductance L_i are expressed as follows (Rahman and Chakravarty 2018; Cottone 2011; Kim et al. 2010; Miller et al. 2016):

$$\alpha = \frac{Bl}{R_L} \quad (25)$$

$$\omega_c = \frac{R_L}{L_i} \quad (26)$$

$$\delta_c = Bl \quad (27)$$

$$L_i = \frac{\mu_0 N^2 \pi {r_c}^2}{h_c} \quad (28)$$

where B is the magnetic flux density, l is the length of wire in the coil, N is the number of turns in the coil, μ_0 is the permeability of the coil material, r_c is the coil radius, and h_c is the coil height.

Electrostatic Equations

The maximum power output expression for the ES mechanism $P_{ES}(\omega)$ at the resonance frequency (Cottone 2011) is given by,

$$|P_{ES}(\omega)| = \frac{Y_0^2}{2}\frac{d_e{m_{eff}}^2{\omega_n}^4\omega^2}{\left(k_{eff} - m_{eff}\omega^2\right)^2 + (d_e + d_m)^2\omega^2} \quad (29)$$

In eq. (29), the mechanical damping d_m and the electrical damping d_e can be expressed as,

$$d_m = 2\zeta_n m_{eff}\omega_n \quad (30)$$

$$d_e = \frac{F_e}{Y_o\omega_n} \quad (31)$$

where the electric force F_e can be given by,

$$F_e = \frac{\varepsilon_0 A_c V^2}{2d_c^2} \quad (32)$$

where ε_0 is the permittivity at free space, A_c is the overlap area of the comb electrodes, and d_c is the gap between two electrodes.

Combined Power Output and Efficiency

The combined maximum power output $P_{combined}$ is not simply the sum of all the stand-alone outputs because the damping of the system causes power loss P_{loss}. Therefore, the total power output combining all the generators is determined by

$$P_{combined} = P_{out} - P_{loss} \quad (33)$$

where the total power output P_{out} is given by

$$P_{out} = P_{PV} + P_{PE}(\omega) + P_{EM}(\omega) + P_{ES}(\omega) \quad (34)$$

The power loss due to the mechanical and electrical damping (Xu et al. 2017) of the hybrid system can be calculated by

$$P_{loss} = P_D + P_{Coil} + P_{Electrodes} \quad (35)$$

In eq. (35), the average power losses P_D, P_{Coil}, and $P_{Electrodes}$ due to the mechanical damping d_m, internal

resistance of the coil R_{Coil}, and internal resistance of variable capacitance electrodes $R_{Electrodes}$, respectively, are expressed as

$$P_D = \frac{1}{2} d_m \omega_n^2 Y_0^2 \tag{36}$$

$$P_{Coil} = P_{EM}(\omega) \frac{R_{Coil}}{R_L} \tag{37}$$

$$P_{Electrodes} = P_{ES}(\omega) \frac{R_{Electrodes}}{R_L} \tag{38}$$

The bias input $P_{in,ES}$ for the ES mechanism, which is supplied by either the battery or the PV panel to the C_{var} electrodes, should be considered as an input while calculating the efficiency of the HEH. If the input power P_{in} is a sum of the $P_{in,ES}$, solar power input, and vibratory power input, then the overall efficiency η of the HEH (Miller et al. 2016) becomes,

$$\eta = \frac{P_{Combined}}{P_{in}} = \frac{P_{Combined}}{P_{solar} + P_{vib} + P_{in,ES}} \times 100\% \tag{39}$$

The magnitude of the vibrational power input P_{vib} is calculated as follows (Rahman 2016; Rahman and Chakravarty 2018), i. e.

$$P_{vib} = \frac{1}{2} m_{eff} g Y_o \omega_n \tag{40}$$

The solar power input P_{solar} is given by,

$$P_{solar} = \lambda A_{PV} = \frac{P_{PV}}{\eta_{Solar}} \tag{41}$$

where λ is the irradiance and A_{PV} is the effective photovoltaic area.

Model Validation with Finite Element Analysis

Fundamental Natural Frequency

The fundamental natural frequency ω_n of the proposed HEH is found 37.16 Hz by eq. (22). Since the power output of the HEH is sensitive to the natural frequency ω_n, finite element (FE) modeling is conducted in ANSYS Workbench 15.0 to verify the analytical result for ω_n. The FE analysis result for ω_n of the HEH is found 35.867 Hz with a deviation of 3.48 % as compared to the analytical result. Figure 8 shows the first resonant mode shape of the HEH obtained by the FE analysis which indicates a good agreement with the first normalized mode shape of a typical cantilever beam with a tip mass (Rahman 2016; Rahman and Chakravarty 2018).

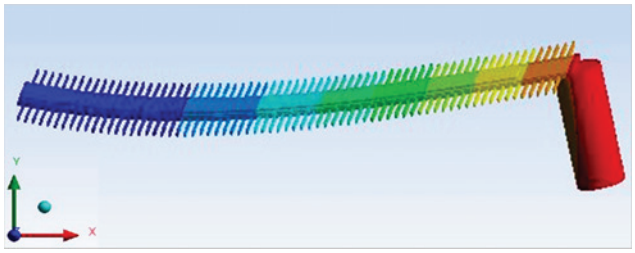

Figure 8: First mode shape of the hybrid cantilever beam with tip mass at ω_n = 35.866 Hz.

Based on the fundamental natural frequency, a mesh independence or, convergence study is conducted using ANSYS where the value of ω_n converges to 35.867 Hz with the increase of degrees of freedom. Figure 9(a) depicts the default converged 3-D mesh of the hybrid beam where 38,402 elements are connected with 121,087 nodes. The convergence of the value of ω_n with the number of nodes is shown in Figure 9(b).

Stress and Fatigue Analysis

Stress and fatigue analyses of the HEH are also done in ANSYS Workbench 15.0 to study the stress and failure criteria of the hybrid structure. The maximum bending stress σ of the beam is found 2.939 MPa analytically following the equation $\sigma = Mc/I_c$ where $c = h_p + h_s/2$ (Rahman 2016). The FE analysis result for the bending stress is found 2.868 MPa which substantiated the accuracy of the analytical calculation by yielding 2.12 % deviation. A fatigue analysis is also done in ANSYS for the substrate material, i. e. Aluminum, since it is clamped to the base, carries the PZT layers (which are not clamped to the base, starts from 0.1 mm on the substrate), Cu electrodes, and tip magnet, and undergoes the maximum stress at the root. Using a fully reversed cyclic load of $F = m_{eff}$. g = 0.10455 N at the tip, a fatigue life of nearly 10^7 cycles is found following the Goodman stress-life approach. Figure 10 shows the distribution of bending stress and

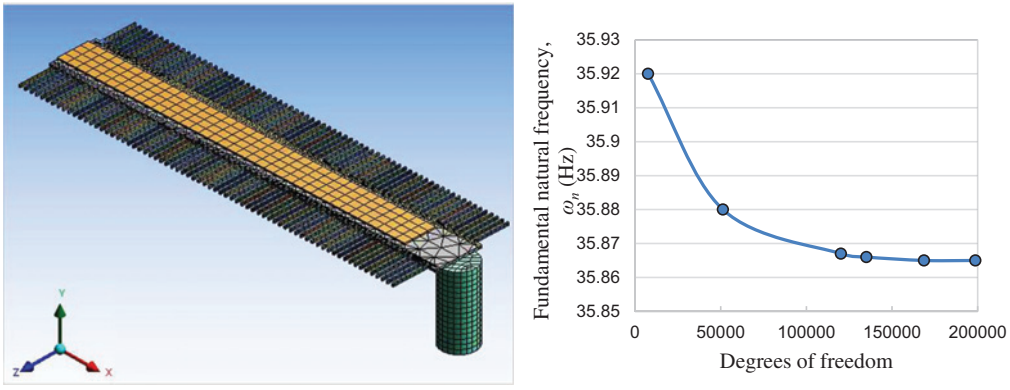

(a) (b)

Figure 9: (a) Computational mesh of the hybrid beam and, (b) Convergence of ω_n value with the increase of DOF.

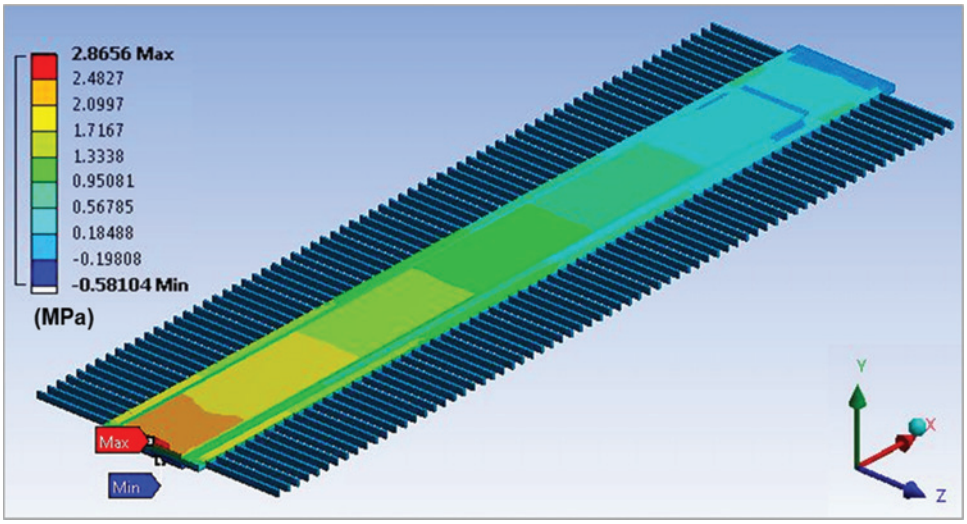

Figure 10: Distribution of stress on the hybrid beam due to tip loading.

its maximum value at the fixed end of the hybrid cantilever beam which is obtained from the FE analysis in ANSYS Workbench.

Results and Discussion

Power and Optimum Load Resistance at the Resonance

The results for the output power of the HEH are obtained in MATLAB R2015a following the mathematical model. The parameters considered for the analytical calculation and numerical simulation are listed in Table 3.

The PV power output along with the *I-V* characteristics is obtained by developing a MATLAB algorithm based on the maximum power point tracking (MPPT) technique at an irradiance level of 1000 W/m^2 (AM 1.5) at 25 °C temperature (Rahman, Sarker, and Chakravarty 2019). Figure 11 shows the maximum power output from the PV panel along with the *I-V* characteristics as obtained from the MPPT algorithm.

The calculations for PE, EM, and ES power outputs are done considering 1 g harmonic base excitation which shown in Figure 12.

The peak of the output power for the PE, EM, and ES generators occurred at resonance, i. e. the fundamental natural frequency ω_n which is found 37.16 Hz. The power outputs around the resonance frequency bandwidth for the PE, EM, and ES methods are shown in Figure 13.

The optimal load resistance is considered as 180 kΩ for the maximum PE output at 37.16 Hz. This is shown in Figure 14 where the resistance at the peak power is the optimal load resistance.

Table 3: Parameters considered for analytical calculation and simulation.

Parameter	Value	Parameter	Value	Parameter	Value
ε_0	8.854×10^{-12} F/m	L	0.1 m	k_{eff}	581.26 N/m
F_e	5.534×10^{-5} N	L_p	0.09 m	δ_c	47.518 Tm
B	1.1 T	L_i	0.0171 H	ω_c	1.05×10^{7}
μ_0	1.257×10^{-6} H/m	R_{Coil}	67.2 Ω	α	2.6×10^{-4}
R_L	180 kΩ	$R_{Electrode}$	12.5 Ω	Y_0	1.8×10^{-4} m
C_p	1.16×10^{-8} F	N	2000	d_e	1.274×10^{-3} kg/s
F_n	4.56 N	r_c	0.0052 m	d_m	0.099 kg/s
M_t	0.0082 kg	r_m	0.0042 m	b_s	0.01 m
m_L	0.0104 kg	h_c	0.025 m	b_p	0.008 m
ρ_e	8960 kg/m^3	h_m	0.020 m	b_e	0.0029 m
ρ_m	7400 kg/m^3	h_s	0.00075 m	χ_n	7.9×10^{-5}
ρ_p	7800 kg/m^3	h_p	0.00040	ζ_n	0.02
ρ_s	2700 kg/m^3	d	0.001 m	φ_n	7.9×10^{-5}

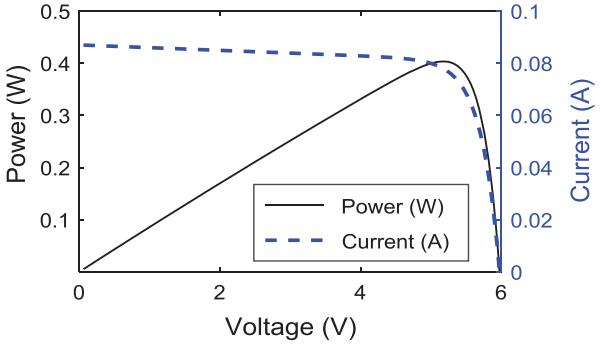

Figure 11: Power output from the PV panel.

In general, energy harvesters are designed to operate in the fundamental natural frequency, i. e. the first mode of vibration which typically provides the maximum deflection and therefore gives the maximum electrical energy (Rahman and Chakravarty 2018). Erturk and Inman (2008, 2009) mentioned that the sign of the mode shapes of a cantilever beam during vibration is analogous to the sign of axial strain distribution along the length and any change in sign reduces the output voltage (Rahman and Chakravarty 2018). As the first mode shape does not change its sign (i. e. stays at one side of the x axis), the corresponding axial strain curve also remains unchanged in its sign. This ensures the maximum voltage generation by the PZT layers. Therefore, strong emphasis is given on determining the fundamental natural frequency and the first mode shape of the structure before calculating the power output and efficiency.

Calculation of Total Power Output and Efficiency

The efficiency of the HEH is determined by eq. (39). The magnitude of P_{vib} is found 2196 μW for 1 g base excitation. On the other hand, considering 17 % efficiency and an irradiance level of 1000 W/m^2 at AM 1.5, the solar energy input P_{solar} yielded a value of 2.35 W. 10 % of the PV power output is utilized for biasing the ES mechanism. The alternate way to provide the bias input for the ES generator is to use the low voltage battery of the circuit. In that case, the rated amount of PV output, i. e. 0.4 W is harvested which contributes to its maximum efficiency. The total power loss due to damping of the system is

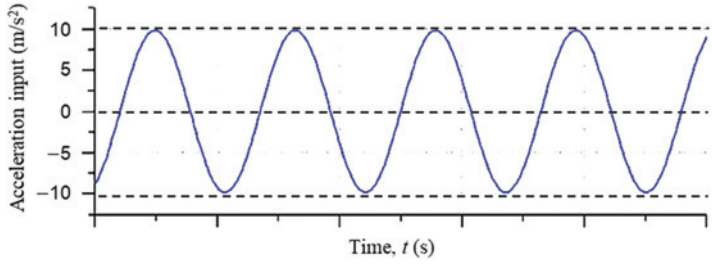

Figure 12: Harmonic base excitation with 1 g (9.81 m/s^2) amplitude.

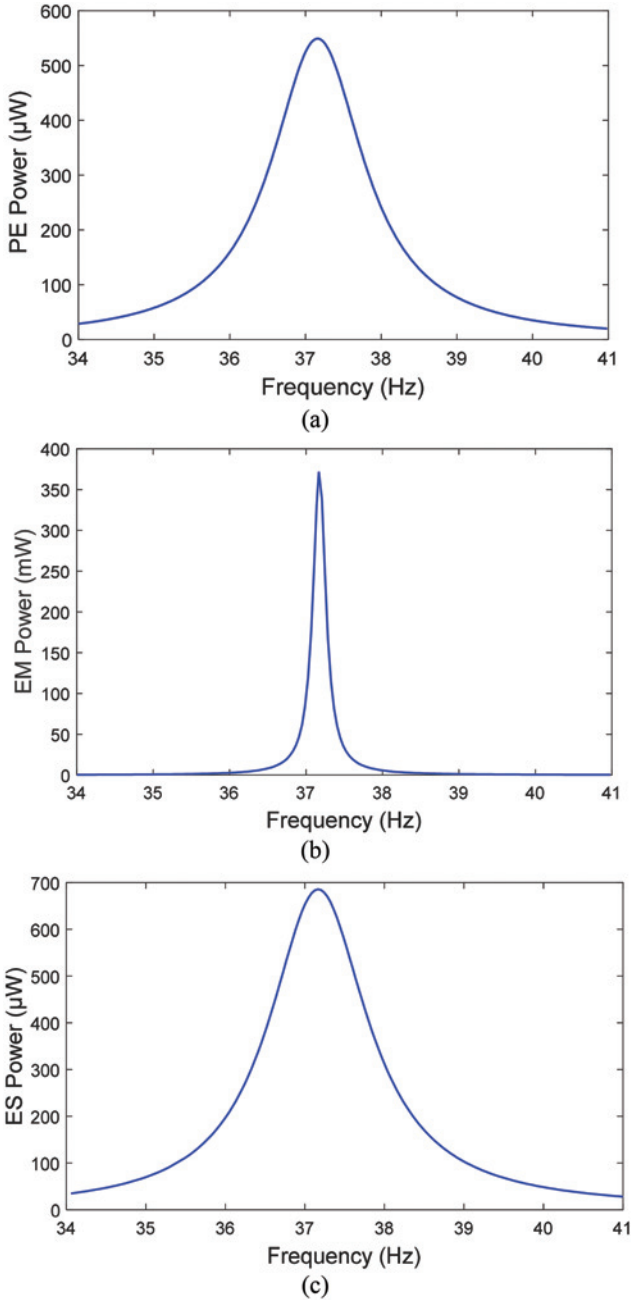

Figure 13: Power outputs at the optimum load resistance from the three vibration-based standalone mechanisms: (a) PE, (b) EM, and (c) ES.

calculated by using eqs. (36)–(38). The power inputs and the total amount of power loss are shown in Figure 15.

The total power output of the HEH is determined by adding all the stand-alone power outputs and deducting the power losses from that amount. While calculating the efficiency, the total input power is considered as the summation of the solar input, base excitation input, and the initial bias input to the ES generator. First, it is assumed that the bias input for the ES generator is supplied by the battery

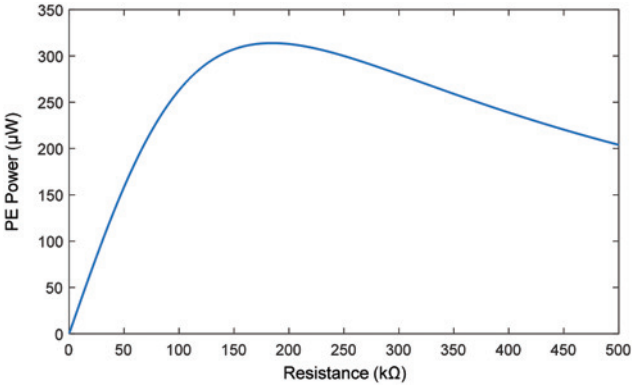

Figure 14: Optimal load resistance R_L at resonance.

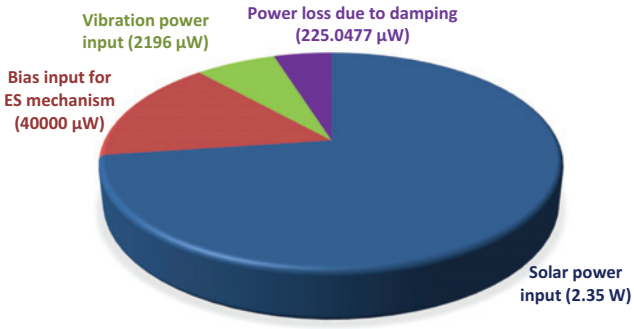

Figure 15: Amounts of input power and power loss for the hybrid energy harvester.

through the microcontroller. The total power output of the HEH in that case is found 772.972 mW with an overall efficiency of 32.3 %, which is greater than the stand-alone power outputs of the PV, PE, EM, and ES generators. The results are shown in Figure 16.

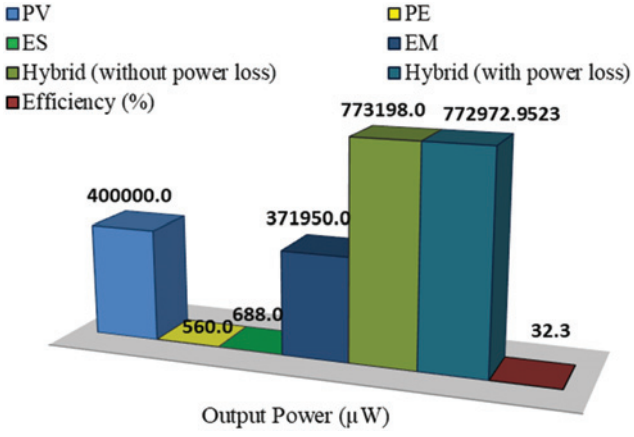

Figure 16: Results for power outputs and efficiency (%) with biasing by the battery.

Instead of the battery, if the PV panel provides 40,000 μW solar power for biasing the ES generator, the total power output of the HEH drops slightly due to the lack of PV power output. In that case, efficiency of the PV panel decreases to 15.3 % and the total power output becomes 732.973 mW with an overall efficiency of 30.6 %. This is illustrated in Figure 17.

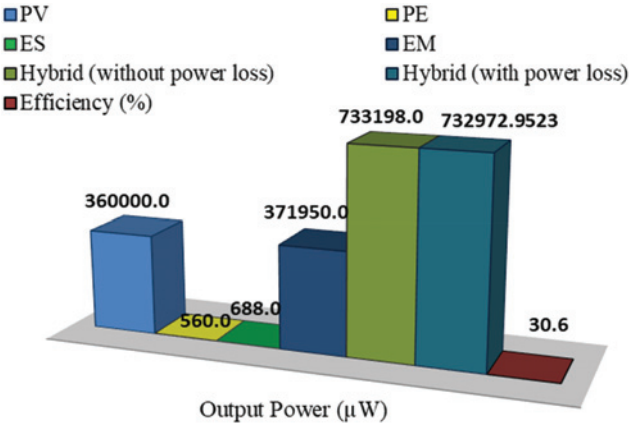

Figure 17: Results for power outputs and efficiency (%) with biasing by the solar panel.

Results displayed in Figures 16 and 17 indicate that the PV and EM generators are the major contributors in the total power output. Results also indicate that, if the battery or the PV panel fails to supply the bias input, the EM generator will still be able to provide the bias input to the ES generator in order to maintain a continuous power transduction.

Effect of Change in Scale of the Beam

Since the fundamental natural frequency ω_n plays an important role in the performance of the vibration energy harvesters, the effects of change in scale or size of the harvester are studied considering the value of ω_n. A parametric study is conducted to observe the effects of change in length and width on the natural frequency of the beam and the total power output from the PE, EM, and ES generators. As the expression for the ω_n suggests, the increases in length L and mass m_{eff} result in the decrease in the value of ω_n for a constant width and thickness. Figures 18 shows the effect of changing length on the fundamental natural frequency of the beam.

On the other hand, at a given length and thickness, the fundamental natural frequency increases with the increase of width of the beam. This effect is illustrated

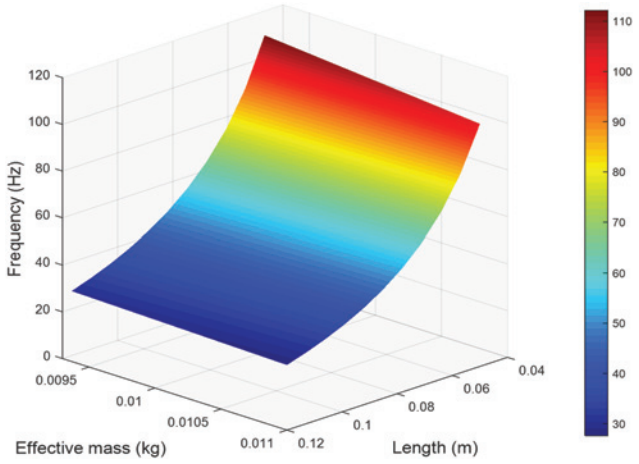

Figure 18: Effect of change in length on the fundamental natural frequency of the beam.

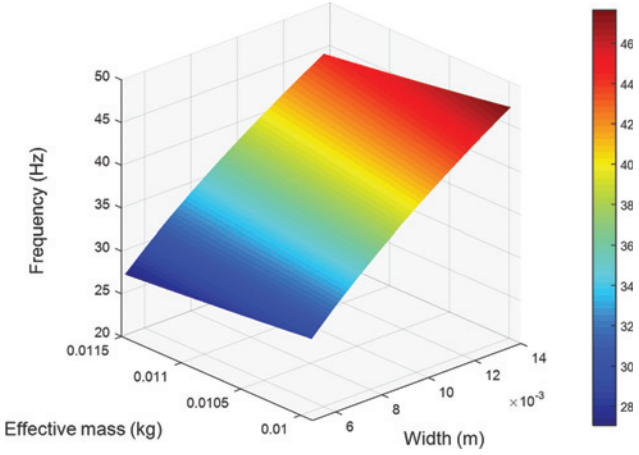

Figure 19: Effect of change in width on the fundamental natural frequency of the beam.

in Figure 19 where the additional width increases the effective mass of the beam but contributes to the increase of the fundamental natural frequency value by increasing the area moment of inertia.

Knowing the variation of natural frequency with the structural parameters is also critical for tuning the vibration energy harvesters. For a given input excitation, any change in natural frequency as a result of adjusting the tip mass or changing the scale, can change the power output of the energy harvester (Rahman 2016). Therefore, it is necessary to optimize the length and width of the beam depending on the value of the fundamental natural frequency. The variations of natural frequency and power output with the change in length and effective width at a given thickness of the vibration-based generators (i. e. PE, EM, and ES generators) are shown in Table 4.

Table 4: Power output from the vibration-based generators at different scales.

Case	Length (m)	Effective width (m)	Thickness (m)	Effective mass (Kg)	Natural frequency (Hz)	PE + EM + ES power output (mW)
1	0.1	0.006	0.00155	0.00994	29.170	125.37
	0.1	0.01	0.00155	0.01066	37.167	373.15
	0.1	0.015	0.00155	0.01156	44.176	378.52
2	0.6	0.01	0.00155	0.00963	84.14	51.40
	0.8	0.01	0.00155	0.01014	53.246	225.35
	0.12	0.01	0.00155	0.011173	27.615	378.56

As mentioned earlier, the size of the PV panel (also the number of arrays) can be adjusted based on the power requirement. The design of the HEH is very flexible in incorporating any small-size PV panel as it is externally connected to the vibration-based system.

Conclusions

In this paper, a self-energized hybrid solar and vibration energy harvester is designed and its performance for a standard base excitation and irradiance level is investigated. Physical and mathematical models of the hybrid structure are presented with illustrations. The proposed hybrid device generates more power than the stand-alone energy harvesters with decent efficiency. In absence of solar energy, the electrostatic components can still obtain the initial bias input from the energy storage or the harvested power with the help of a microcontroller which implies that failure of one generator will not result in disruption of the entire power generation. The proposed design thus, ensures a simultaneous harvesting of energy and a continuous supply of power to the low-powered electronic components. The reciprocal interactions (e. g. electromechanical damping) of the mechanisms are handled by considering a reasonable value of damping of the hybrid system. While calculating the actual power output, considering the effect of damping is important because the material damping, surrounding air damping, internal resistances of the coil, and electrostatic action of the electrodes cause a power loss during the hybrid power generation. The effect of changing scale of the geometry on the performance of the hybrid device is also studied.

A finite element analysis is also done to validate the model and investigate the fatigue behavior of the structure. The analytical results for the fundamental frequency and bending stress show a good agreement with the finite element analysis results. The results for the expected life and potential failure zone of the aluminum substrate are quite reasonable compared to the standard S-N curves. Overall, the coupled electromechanical model, combined circuit, and finite element analysis presented in this study facilitate the knowledge and development of an efficient hybrid energy harvester for meeting the growing demand of power management for wireless sensors and microelectromechanical systems.

Conflict of Interest: There is no conflict of interest in this work. However, the authors are thankful to Bikrant Poudel from the Department of Electrical Engineering, University of New Orleans for his cooperation and electrical engineering concepts.

Funding: The authors received no financial support for this research.

References

Ahmed, R., F. Mir, and S. Banerjee. 2017. "A Review on Energy Harvesting Approaches for Renewable Energies from Ambient Vibrations and Acoustic Waves Using Piezoelectricity." *Smart Materials and Structures* 26 (085031): 1–33.

Al-Haik, M., A. Alothman, and M. Hajj. 2018. "Integrated Thermoelectric Energy Generator and Organic Storage Device." *Energy Harvesting and Systems* 5 (3–4): 73–79.

Arnold, D. P. 2007. "Review of Microscale Magnetic Power Generation." *IEEE Transactions on Magnetics* 43: 3940–3951.

Beeby, S. P., M. J. Tudor, and N. M. White. 2006. "Energy Harvesting Vibration Sources for Microsystems Applications." *Measurement Science and Technology* 13: R175–95.

Castagnetti, D. 2011. "Fractal-Inspired Multifrequency Structures for Piezoelectric Harvesting of Ambient Kinetic Energy." *ASME Journal of Mechanical Design* 133 (11): 111005:1–8.

Challa, V. R., M. G. Prasad, and F. T. Fisher. 2009. "A Coupled Piezoelectric–electromagnetic Energy Harvesting Technique for Achieving Increased Power Output through Damping Matching." *Smart Materials and Structures* 18 (005029): 1–11.

Challa, V. R., M. G. Prasad, and F. T. Fisher. 2011. "Towards an Autonomous Self-tuning Vibration Energy Harvesting Device for

Wireless Sensor Network Application." *Smart Materials and Structures* 20 (025004): 1–11.

Chavez, L., F. Zayas Jimenez, B. Wilburn, L. C. Delfin, H. Kim, N. Love, and Y. Lin. 2017. "Characterization of Thermal Energy Harvesting Using Pyroelectric Ceramics at Elevated Temperatures." *Energy Harvesting and Systems* 5 (1–2): 3–10.

Chen, W., Y. Cao, and J. Xie. 2015. "Piezoelectric and Electromagnetic Hybrid Energy Harvester for Powering Wireless Sensor Nodes in Smart Grid." *Journal of Mechanical Science and Technology* 29 (10): 4313–18.

Chen, Z. S., Y. M. Yang, and G. Q. Deng. 2009. "Analytical and Experimental Study on Vibration Energy Harvesting Behaviors of Piezoelectric Cantilevers with Different Geometries." *International Conference on Sustainable Power Generation and Supply* Nanjing, China: IEEE, pp.1–6.

Colomer-Farrarons, J., P. Miribel-Catala, A. Saiz-Vela, and J. Samitier. 2011. "A Multiharvested Self-Powered System in A Low-Voltage Low-Power Technology." *IEEE Transactions on Industrial Electronics* 58 (9): 4250–63.

Cottone, F. 2011, "Introduction to Vibration Energy Harvesting." Retrieved from http://wwwnipslab.org/files/file/nips%20summer%20school%202011/Cottone%20Introduction%20to%20vibration%20harvesting.pdf.

Cui, Y., Q. Y. Zhang, M. L. Yao, W. J. Dong, and S. Q. Gao. 2015. "Vibration Piezoelectric Energy Harvester with Multi-beam." *AIP Advances* 5: 041332–9.

Davidson, J., and C. Mo. 2014. "Recent Advances in Energy Harvesting Technologies for Structural Health Monitoring Applications." *Smart Materials Research* 2014 (410316): 1–14.

De Pasquale, G., A. Somà, and F. Fraccarollo. 2012. "Piezoelectric Energy Harvesting for Autonomous Sensors Network on Safety-improved Railway Vehicles." *Proceedings of the Institution of Mechanical engineers, Part C: Journal of Mechanical Engineering Science* 226 (4): 1107–1117.

Edwards, B., K. C. Aw, and A. P. Hu. 2015. "Hybrid Electromagnetic-piezoelectric Transduction for a Frequency Up-converted Energy Harvester." IEEE International Conference on Advanced Intelligent Mechatronics, pp. 1149–54.

Erturk, A., and D. J. Inman. 2008. "On Mechanical Modeling of Cantilevered Piezoelectric Vibration Energy Harvesters." *Journal of Intelligent Material Systems and Structures* 19: 1311–1325.

Erturk, A., and D. J. Inman. 2009. "An Experimentally Validated Bimorph Cantilever Model for Piezoelectric Energy Harvesting from Base Excitations." *Smart Materials and Structures* 18 (025009): 1–18.

Eun, Y., D. Kwon, M. Kim, I. Yoo, J. Sim, H. Ko, K. Cho, and J. Kim. 2014. "A Flexible Hybrid Strain Energy Harvester Using Piezoelectric and Electrostatic Conversion." *Smart Materials and Structures* 23 (045040): 1–6.

Gambier, P., S. R. Anton, N. Kong, A. Erturk, and D. J. Inman. 2012. "Piezoelectric, Solar and Thermal Energy Harvesting for Hybrid Low-power Generator Systems with Thin-film Batteries." *Measurement Science and Technology* 23 (01510): 1–11.

Glynne-Jones, P., M. J. Tudor, S. P. Beeby, and N. M. White. 2004. "An electromagnetic, Vibration-powered Generator for Intelligent Sensor Systems." *Sensors and Actuators A* 110: 344–49.

Goudarzi, M., K. Niazi, and M. K. Besharati. 2013. "Hybrid Energy Harvesting from Vibration and Temperature Gradient by PZT and PMN-0.25PT Ceramics." *Materials Physics and Mechanics* 16: 55–65.

Grover, M., M. Nehra, and D. Kedia. 2019. "Simulative Parametric Study on Heterojunction Thin Film Solar Cells Incorporating Interfacial Nanoclusters Layer." *Energy Harvesting and Systems* 6 (1–2): 23–28.

Hwang, G. T., M. Byun, C. K. Jeong, and K. J. Lee. 2015. "Flexible Piezoelectric Thin-film Energy Harvesters and Nanosensors for Biomedical Applications." *Advanced Healthcare Materials* 4: 646–658.

Jiang, X., J. Wang, Y. Li, J. Li, and J. Yao. 2015. "Energy Harvesting for Powering Wireless Sensor Networks in Low-frequency and Large-force Environments." *Proceedings of the Institution of Mechanical Engineers, Part C: Journal of Mechanical Engineering Science* 229 (11): 1953–1964.

Kang, M. G., W. S. Jung, C. Y. Kang, and S. J. Yoon. 2016. "Recent Progress on PZT Based Piezoelectric Energy Harvesting Technologies." *Actuators* 5 (5): 1–17.

Khaligh, A., P. Zeng, and C. Zheng. 2010. "Kinetic Energy Harvesting Using Piezoelectric and Electromagnetic technologies—State of the Art." *IEEE Transactions on Industrial Electronics* 57: 850–860.

Khan, F. U., and Izhar. 2016. "Hybrid Acoustic Energy Harvesting Using Combined Electromagnetic and Piezoelectric Conversion." *Review of Scientific Instruments* 87 (025003): 1–10.

Khan, F. U., and M. U. Qadir. 2016. "State-of-the-art in Vibration-based Electrostatic Energy Harvesting." *Journal of Micromechanics and Microengineering* 26: 103001–28.

Khbeis, M., J. McGee, and R. Ghodssi. 2009. "Development of a Simplified Hybrid Ambient Low Frequency Low Intensity Vibration Energy Scavenger System." Transducers 2009, Denver, CO, pp. 525–28.

Kim, J., F. Cottone, S. Goyal, and J. Punch. 2010. "Energy Scavenging for energy Efficiency in Networks and Applications." *Bell Labs Technical Journal* 15: 7–29.

Larkin, M., and Y. Tadesse. 2013. "HM-EH-RT: Hybrid Multimodal Energy Harvesting from Rotational and Translational Motions." *International Journal of Smart and Nano Materials* 4: 257–85.

Lee, J., J. Kim, T. Kim, M. A. Hossain, S. Kim, and J. Kim. 2016. "All-in-one Energy Harvesting and Storage Devices." *Journal of Materials Chemistry A* 4 (21): 7983–99.

Lee, S., and A. Tovar. 2013. "Topology Optimization of Piezoelectric Energy Harvesting Skin Using Hybrid Cellular Automata." *ASME Journal of Mechanical Design* 135 (3): 031001:1–11.

Lewis, J., J. Zhang, and X. Jiang. 2009. "Fabrication of Organic Solar Array for Applications in Micro-electromechanical Systems." *Journal of Renewable and Sustainable Energy* 1 (013101): 1–8.

Liu, H., S. Wang, Y. Zhang, and W. Wang. 2015. "Study on the Giant Magnetostrictive Vibration-power Generation Method for Battery-less Tire Pressure Monitoring System." *Proceedings of the Institution of Mechanical engineers, Part C: Journal of Mechanical Engineering Science* 229 (9): 1639–1651.

Luo, Y., R. Gan, S. Wan, R. Xu, and H. Zhou. 2016. "Design and Analysis of a MEMS-based Bifurcate-shape Piezoelectric Energy Harvester." *AIP Advances* 6 (045319): 1–9.

Madinei, H., H. H. Khodaparast, S. Adhikari, and M. I. Friswell. 2016. "A Hybrid Piezoelectric and Electrostatic Vibration Energy Harvester." Conference Proceedings of the Society for Experimental Mechanics Series. In *Shock & Vibration, Aircraft/*

Aerospace,Energy Harvesting, Acoustics & Optics, Vol. 9, edited by A. Brandt, and R. Singhal, 189–195. Cham: Springer.

Miles, R. W., K. M. Hynes, and I. Forbes. 2005. "Photovoltaic Solar Cells: an Overview of State-of-the-art Cell Development and Environmental Issues." *Progress in Crystal Growth and Characterization of Materials* 51: 1–42.

Miller, L. M., A. D. T. Elliott, P. D. Mitcheson, E. Halvorsen, I. Paprotny, and P. K. Wright. 2016. "Maximum Performance of Piezoelectric Energy Harvesters When Coupled to Interface Circuits." *IEEE Sensors* 16 (12): 4803–15.

Mitcheson, P., P. Miao, B. Start, E. Yeatman, A. Holmes, and T. Green. 2004. "MEMS Electrostatic Micro-Power Generator for Low Frequency Operation." *Sensors and Actuators A* 115: 523–29.

Moss, S. D., O. R. Payne, G. A. Hart, and C. Ung. 2015. "Scaling and Power Density Metrics of Electromagnetic Vibration Energy Harvesting Devices." *Smart Materials and Structures* 24 (023001): 1–14.

Priya, S., H. Song, Y. Zhou, R. Varghese, A. Chopra, S. Kim, I. Kanno, L. Wu, D. S. Ha, J. Ryu, and R. G. Polcawich. 2017. "A Review on Piezoelectric Energy Harvesting: Materials, Methods, and Circuits." *Energy Harvesting and Systems* 4 (1): 3–39.

Rahman, M. S. 2016. "A Hybrid Technique of Energy Harvesting from Mechanical Vibration and Ambient Illumination." Master's thesis, Louisiana, USA: University of New Orleans.

Rahman, M. S., and U. K. Chakravarty. 2018. "A Hybrid Energy Harvesting System Based on Solar Radiation and Mechanical Vibration." *Proceedings of. ASME 2018 International Mechanical Engineering Congress & Exposition*, Vol. 1, Advances in Aerospace Technology, Pittsburgh, Pennsylvania, USA, pp. 1–12.

Rahman, M. S., P. Sarker, and U. K. Chakravarty. 2019. "A Hybrid Energy Harvester Based on Solar Radiation and Mechanical Vibration." *AIP Conference Proceedings* 2121 (1): 120008:1–6.

Rantz, R., and S. Roundy. 2017. "Characterization of Real-world Vibration Sources and Application to Nonlinear Vibration Energy Harvesters." *Energy Harvesting and Systems* 4 (2): 67–76.

Roundy, S. 2003. "Energy Scavenging for Wireless Sensor Nodes with a Focus on Vibration to Electricity Conversion." Ph.D. thesis, Berkeley: University of California.

Roundy, S., P. Wright, and J. Rabaey. 2003. *Energy Scavenging for Wireless Sensor Networks*. Boston: Kluwer Academic Publishers.

Sample, A., and J. R. Smith. 2009. "Experimental Results with Two Wireless Power Transfer Systems." IEEE Radio and Wireless Symposium, San Diego, CA, pp. 16–18.

Shan, X. B., S. W. Guan, Z. S. Liu, Z. L. Xu, and T. Xie. 2013. "A New Energy Harvester Using A Piezoelectric and Suspension Electromagnetic Mechanism." *Journal of Zhejiang University-Science A (Applied Physics and Engineering)* 14 (12): 890–97.

Sharma, H., A. Haque, and Z. A. Jaffery. 2018. "Solar Energy Harvesting Wireless Sensor Network Nodes: A Survey." *Journal of Renewable and Sustainable Energy* 10 (2): 023704:1–33.

Sivula, K. 2015. "Toward Economically Feasible Direct Solar-to-fuel Energy Conversion." *The Journal of Physical Chemistry Letters* 6: 975–976.

Sood, V. K., and P. Bhalla. 2013. "EMTP Model of Grid Connected PV System." *Proceedings of International Conference on Power System Transients*, Vancouver, Canada, pp. 1–8.

Su, D., R. Zheng, K. Nakano, and M. P. Cartmell. 2016. "Stabilisation of the High Energy Orbit for a Nonlinear energy Harvester with Variable Damping." *Proceedings of the Institution of Mechanical engineers, Part C: Journal of Mechanical Engineering Science* 230 (12): 2003–2012.

Tao, K., J. Miao, S. Lye, and X. Hu. 2015. "Sandwich-structured Two-dimensional MEMS Electret Power Generator for Low-level Ambient Vibrational Energy Harvesting." *Sensors and Actuators A: Physical* 228: 95–103.

Wang, T., T. Kobayashi, and C. Lee. 2015. "Micromachined Piezoelectric Ultrasonic Transducer with Ultra-wide Frequency Bandwidth." *Applied Physics Letters* 106: 013501–5.

Waterbury, A. C., and P. K. Wright. 2013. "Vibration Energy Harvesting to Power Condition Monitoring Sensors for Industrial and Manufacturing Equipment." *Proceedings of the Institution of Mechanical engineers, Part C: Journal of Mechanical Engineering Science* 227 (6): 1187–1202.

Wurpts, W., J. Twiefel, and F. Brouet. 2017. "Equivalent Circuit Parametrization Utilizing FE Model Order Reduction and Its Application to Piezoelectric Generators and Actuators." *Energy Harvesting and Systems* 4 (3): 115–129.

Xu, Z., X. Shan, D. Chen, and T. Xie. 2016. "A Novel Tunable Multi-Frequency Hybrid Vibration Energy Harvester Using Piezoelectric and Electromagnetic Conversion Mechanisms." *Applied Science* 6 (10): 1–16.

Xu, Z., X. Shan, H. Yang, W. Wang, and T. Xie. 2017. "Parametric Analysis and Experimental Verification of a Hybrid Vibration Energy Harvester Combining Piezoelectric and Electromagnetic Mechanisms." *Micromachines* 8 (189): 1–19.

Yang, B., C. Lee, L. W. Kee, and P. S. Lim. 2010. "Hybrid Energy Harvester Based on Piezoelectric and Electromagnetic Mechanisms." *Journal of Micro/Nanolithography, MEMS and MOEMS* 9 (023002): 1–10.

Yi, J. W., W. Y. Shih, and W. H. Shih. 2002. "Effect of length, width, and Mode on the Mass Detection Sensitivity of Piezoelectric Unimorph Cantilevers." *Journal of Applied Physics* 91: 1680–86.

Yildirim, T., M.H. Ghayesh, T. Searle, W. Li, and G. Alici. 2017. "A Parametrically Broadband Nonlinear Energy Harvester." *ASME Journal of Energy Resources Technology* 139: 032001:1–8.

Yu, H., Q. Yue, J. Zhou, and W. Wang. 2014. "A Hybrid Indoor Ambient Light and Vibration Energy Harvester for Wireless Sensor Nodes." *Sensors* 14: 8740–55.

Yuan, Y., M. Liu, W. Tai, and L. Zuo. 2018. "Design and Treadmill Test of a Broadband Energy Harvesting Backpack with a Mechanical Motion Rectifier." *ASME Journal of Mechanical Design* 140 (8): 085001:1–8.

Zhang, H. 2011. "Power Generation Transducer from Magnetostrictive Materials." *Applied Physics Letters* 98 (232505): 1–7.

Zhang, Y. 2014. "Piezoelectric Based Energy Harvesting on Low Frequency Vibrations of Civil Infrastructures." Ph.D, Baton Rouge, LA: Lousiana State University.

Zhu, J., N. S. Yuksek, M. Almasri, and Z. Feng. 2019. "Numerical Modeling of Dynamic Response of Miniature Multi-impact Electromagnetic Device for Low and Wide Range Frequencies Energy Harvesting." *Proceedings of the Institution of Mechanical engineers, Part C: Journal of Mechanical Engineering Science* 233 (7): 2400–2409.